ORNL/Sub-7327/11

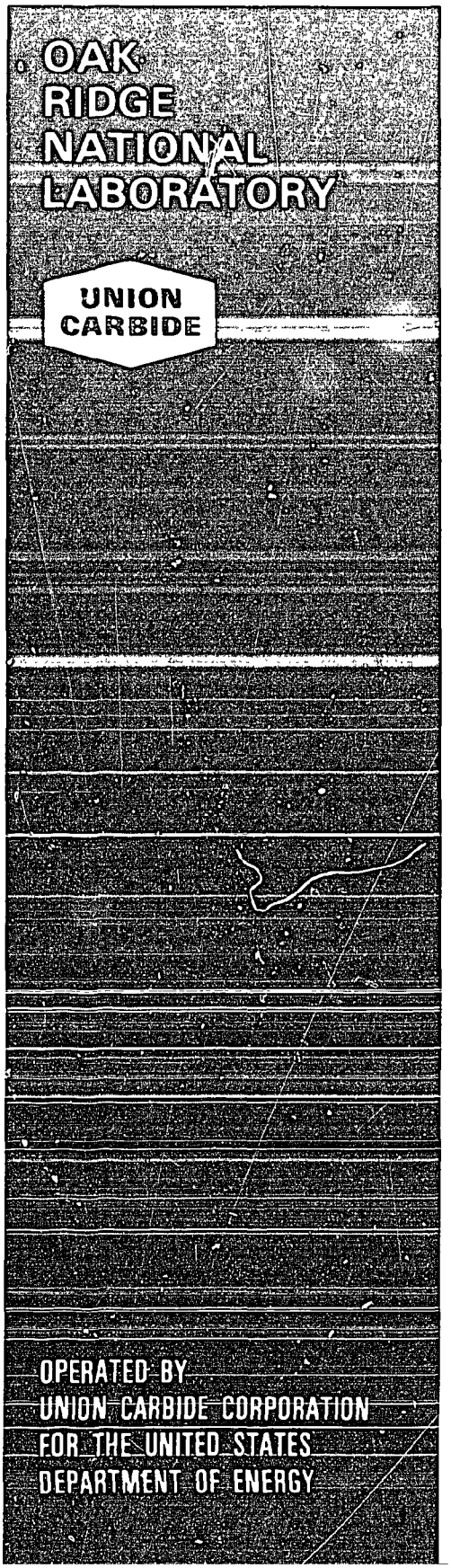

Materials Performance in Off-Gas Systems Containing Iodine

J. A. Beavers
W. E. Berry
J. C. Griess

ORNL/Sub-7327/11
Dist. Category UC-86

Consolidated Fuel Reprocessing Program

MATERIALS PERFORMANCE IN OFF-GAS SYSTEMS CONTAINING IODINE

J. A. Beavers and W. E. Berry
Battelle Columbus Laboratories
Columbus, Ohio

J. C. Griess
Metals and Ceramics Division
Oak Ridge National Laboratory
Oak Ridge, Tennessee

Date Published - November 1981

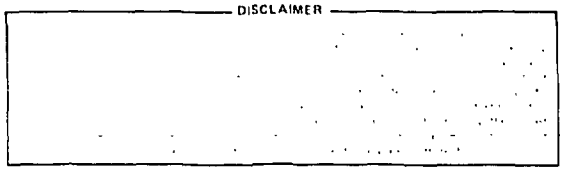

Prepared under Subcontract 7327
for
OAK RIDGE NATIONAL LABORATORY
Oak Ridge, Tennessee 37830
operated by
UNION CARBIDE CORPORATION
for the
U.S. DEPARTMENT OF ENERGY
Contract No. W-7405-eng-26

CONTENTS

MATERIALS PERFORMANCE IN OFF-GAS SYSTEMS CONTAINING IODINE

J. A. Beavers and W. E. Berry
Battelle Columbus Laboratories

J. C. Griess
Oak Ridge National Laboratory

ABSTRACT

During the reprocessing of spent reactor fuel elements, iodine is released to gas streams from which it is ultimately removed by conversion to nonvolatile iodic acid. Under some conditions iodine can produce severe corrosion in off-gas lines; in this study these conditions were established.

Iron- and nickel-based alloys containing more than 6% molybdenum, such as Hastelloy G (7%), Inconel 625 (9%), and Hastelloy C-276 (16%), as well as titanium and zirconium, remained free of attack under all conditions tested. When the other materials, notably the austenitic stainless steels, were exposed to gas streams containing even only low concentrations of iodine and water vapor at 25 and 40°C, a highly corrosive, brownish-green liquid formed on their surfaces. In the complete absence of water vapor, the iodine-containing liquid did not form and all materials remained unaffected. The liquid that formed had a low pH (usually <1), and the attack was about the same in either air or nitrogen. The rate of attack increased with increasing temperature at constant relative humidity but decreased with increasing temperature at constant water content. The severity of attack increased with the increasing water content of the gas except under conditions where relatively large amounts of water were present, such as on a condensing surface. Nitric acid and NO_2 inhibited attack.

1. INTRODUCTION

In the reprocessing of reactor fuel elements, fission-product iodine appears in gas streams and must ultimately be collected. In the conceptual fuel reprocessing flowsheet under development in the Consolidated Fuel Reprocessing Program, iodine in gas streams will be reacted with hyperazeotropic nitric acid and converted to nonvolatile iodic acid, which will be collected for disposal. The voloxidizer, the primary and secondary dissolvers, and the digestion tanks located directly downstream from the primary dissolver are major sources of iodine-containing off-gases in the proposed flowsheet. The off-gas from the voloxidizer will contain, among other constituents, tritiated water and iodine. The tritiated water will be recovered in a molecular sieve bed that will also collect some iodine, and some iodine may crystallize on the cooled surfaces of the voloxidizer off-gas piping system. The off-gas from the primary dissolver and digestion tanks will contain I_2, NO_x, and HNO_3 vapors. If HI is used in the secondary dissolver, it will introduce HI and I_2 vapors into the gas phase; and if the iodine is recovered from the HI as elemental iodine by reaction with dilute HNO_3, NO_x and HNO_3 will also be present in off-gas lines from the secondary dissolver.

The fact that elemental iodine may create serious corrosion problems in the off-gas system was recognized early in the project, but only limited information was available on materials performance in iodine-containing environments. Creek and Griess[1] studied the effect of water and 4 *M* HNO_3 saturated with iodine on the corrosion of materials at room temperature. Severe pitting of type 304L stainless steel (SS) occurred where iodine crystals or an iodine-containing solution was present on the specimen surfaces. The presence of

sufficient molybdenum in iron- and nickel-based alloys markedly increased their corrosion resistance. In addition, Zircaloy-2, titanium, and tantalum also were resistant to attack. Similar results were reported by other researchers, and it was noted that water vapor was necessary for pitting of iron- and nickel-based alloys to occur both at room temperature[2,3] and at elevated temperatures.[4]

The objective of the experimental program described in this report was to evaluate the corrosion performance of candidate materials of construction for off-gas lines in environments that closely simulate those that will be encountered in the fuel reprocessing off-gas system. The study focused on problems associated with elemental iodine in the off-gas.

2. EXPERIMENTAL PROCEDURE

A variety of exposure tests was carried out using unwelded specimens of the candidate materials. Specimens (23.5 mm × 23.5 mm with different thicknesses) were abraded with numbers 250 and 400 SiC, degreased in acetone, and rinsed in distilled water. They were then weighed and exposed for various periods to the simulated off-gas streams. Following exposure, the specimens were evaluated for attack by weight loss and by optical measurements of pit depths, using a microscope with a calibrated stage.

Most tests were carried out in a chamber into which humidified air or nitrogen, iodine vapors, and NO_2 were introduced (designated Apparatus A). Limited exposures were also carried out above HNO_3 solutions (equipment designated Apparatus B and Apparatus C). All components of the equipment were fabricated of Pyrex or Teflon. Descriptions are given below.

2.1 Apparatus A

Apparatus A consisted of four gas flow lines that were combined upstream of a specimen chamber. one line contained water-saturated air; the second, dry air; the third, iodine-saturated air; and the fourth, NO_2. Various concentrations of these components were produced by varying the relative flow rates in the four lines.

The water-saturated air was generated by sparging air through two flasks (connected in series) containing distilled water. The vapors were then passed through a tower packed with glass wool to remove any mist. The dry air was generated by passing air through a tower containing anhydrous $CaSO_4$. The iodine-saturated air was generated by passing dry air through two towers (connected in series) containing iodine crystals. Reagent-grade NO_2 was obtained from a gas cylinder and diluted with dry air before being introduced into the specimen chamber. The flow rate in all four lines was continuously monitored by means of Brooke rotameters. A schematic diagram of the experimental apparatus is shown in Fig. 2.1.

The water-saturated air line was calibrated by passing the gas through two drying towers (connected in series) containing anhydrous $CaSO_4$, which was weighed before and after timed exposure periods. The iodine-saturated air line was calibrated by sparging the gas through two flasks (connected in series) containing 0.06 *M* KI solution. The concentration of iodine trapped by the solution was determined by chemical analysis. The results of these calibrations are given in Table 2.1. The relative humidities at 25 and 40°C were 87 and 78%,

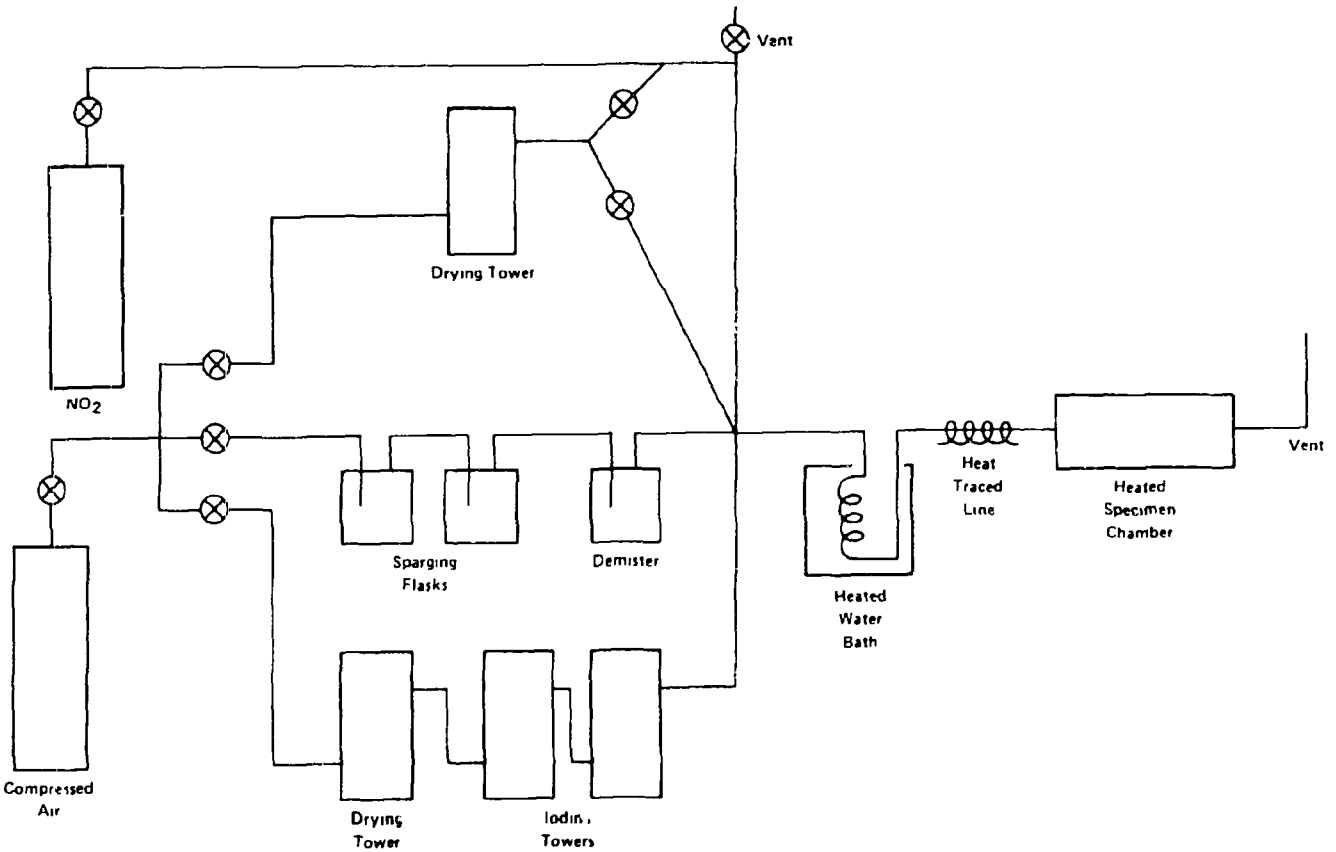

Fig. 2.1. Schematic of Apparatus A.

Table 2.1. Results of calibration tests performed on air containing iodine and water vapor at flow rate of 20 to 40 mL/min

Temperature (°C)	Water		Iodine	
	Concentration (g/mL)	Relative saturation (%)	Concentration (g/mL)	Relative saturation (%)
25	2.0×10^{-5}	87	1.5×10^{-6}	37
40	4.0×10^{-5}	78	4.2×10^{-6}	31

respectively, indicating that the air stream was not completely saturated with water. The same was true for the iodine stream. Based on data reported in the *International Critical Tables*,[5] the iodine concentration of the air, after passing through the iodine beds, was only 37 and 31% saturated at 25 and 40°C respectively. Essentially the same values for both water and iodine were obtained at flow rates of either 20 or 40 mL/min.

The initial testing was carried out with a horizontal cylindrical specimen chamber 7.5 cm in diameter by 45 cm in length. The gases were introduced into one end of the cylinder at a rate of 40 mL/min and passed over the individual specimens located along the axis of the cylinder. When it was found that the rate of attack of identical specimens was a function of position in the chamber, a modified desiccator was substituted for the cylindrical specimen chamber and the flow rate was increased to 80 mL/min. The location effect in the original equipment was related to a reduction in the iodine concentration along the length of the chamber, and the above changes eliminated the problem. All results from tests performed with the horizontal cylindrical chamber are identified in the report.

2.2 Apparatus B

Apparatus B was used to evaluate the influence of acid concentrations on corrosion in subsaturated iodine vapors. It consisted of a 500-mL specimen chamber located above a distilling flask. Cooling coils were positioned beneath the specimen holder in the chamber to cool the specimens to the desired temperature. The off-gases from the distilling flask were passed over the specimens, and any condensed liquid was returned to the distilling flask through a trap located between the two vessels. Inlets were provided to add iodine or NO_2 vapors either by bubbling through the boiling solution or by passing the gas over the solutions.

2.3 Apparatus C

Apparatus C was used to examine the influence of acid concentration, reflux rate, and the presence of crevices on the corrosion of candidate materials in supersaturated iodine vapors. Specimens were attached to the inside diameter of an Allihn condenser connected to a distilling flask containing HNO_3. At the start of the test, 10 g of iodine was added to the boiling solution, resulting in the rapid deposition of elemental iodine onto the specimen surfaces.

2.4 Other tests

Exposure tests were carried out on specimens of type 304L SS in HI containing elemental iodine and in HI containing HNO_3 and elemental iodine. These tests were conducted at 25°C under naturally aerated conditions.

In other studies the electrochemical potential of selected alloys was measured, and the pH of solutions formed when iodine crystals and small volumes of water were placed on metal surfaces was determined. Specimens were abraded with numbers 250 and 400 SiC and rinsed in acetone and distilled water, and the tips of micro-pH and micro-potential electrodes were placed on the surface. A drop of distilled water (0.1 mL) was placed on the specimen surface such that it wetted the tips of both electrodes, and the system was allowed to equilibrate for 20 min. Iodine (0.1 g) was then added to the water droplet, and the pH and potential were measured as a function of time.

2.5 Materials

The materials evaluated in the off-gas study and their nominal compositions are given in Table 2.2.

Table 2.2. Nominal compositions of materials evaluated in the experimental program

Alloy	Composition (wt %)						
	Fe	Ni	Cr	Mo	C	Mn	Other
304L SS	70.0	9	19.0		0.03[a]	2.00[a]	
316L SS	67.0	12	17.0	2.2	0.03[a]	2.00[a]	
317LM SS	66.0	13	17.0	4.0[b]	0.03[a]		
EAS 2 Si	63	15	18.0		0.02[a]		4.0 Si
E-Brite 26-1	7.30		26.0	1.0	0.002	0.10	
AL 29-4	67.0		29.0	4.0	0.003[a]	0.10[a]	
Carpenter 20 Cb-3	37.0	34	20.0	3.0	0.07[a]	2.00[a]	3.5 Cu, 1.0[a] Nb + Ta
Incoloy 800	39.5[b]	33	21.0		0.10[a]	1.5[a]	0.75[a] Cu, 0.4 Al, ~0.4 Ti
Incoloy 825	22.0[b]	42	22.0	3.0	0.05[a]	1.0[a]	2.3 Cu, 0.2[a] Al, 0.9 Ti
Inconel 600	7.2	76.0	16.0		0.04	0.2	0.1 Cu
Inconel 625	5.0[a]	58.0[b]	22.0	9.0	0.10[a]	0.50[a]	3.6 Nb + Ta, 0.40[a] Al, 0.40 Ti
Inconel 671		51.0	48.0		0.05		0.35 Ti
Inconel 690	10.0	60.0	30.0		0.03		
Hastelloy C-276	6.0	56.0	16.0	16.0	0.02[a]	1.0[a]	4 W, 2.5 Co, 0.35[a] V
Hastelloy G	20.0	44.0	22.0	7.0	0.05[a]	1.5	2.5 Co, 2 Nb + Ta, 1 W
CP titanium	0.20				0.08		0.05 N Bal Ti
CP zirconium	0.07	0.03	0.05		0.15		1.90 Hf[a] Bal Zr
Nickel 201	0.15	99.5			0.01	0.2	0.005 S, 0.005 Si, 0.05 Cu
Armco Iron	Bal				0.03		
Electrolytic Chromium			99.0				

[a]Maximum.
[b]Minimum.

3. RESULTS

3.1 Tests in Apparatus A

3.1.1 Effect of alloy composition

The results of 400-h exposure tests performed on 15 candidate materials in air containing iodine and water at 25°C are given in Table 3.1. In these tests the iodine concentration was only 18% saturated and the relative humidity was 46%. These data show that titanium, zirconium, and the molybdenum-containing nickel-based alloys were resistant to attack, whereas the stainless steels and some nickel-based alloys containing no molybdenum experienced significant weight loss and pitting. This group of specimens was exposed in the horizontal cylinder, and observed rates were location dependent.

Table 3.1. Average corrosion rates and average pit depths (three deepest pits) for materials exposed 400 h to air containing 7.4×10^{-7} g/mL of iodine and 1.0×10^{-5} g/mL of H_2O at 25°C[a]

Material	Corrosion rate (μm/year)	Pit depth (μm)	Iodine deposition
Titanium	<2.5 (<0.1)	None	No
Zirconium	<2.5 (<0.1)	None	No
Hastelloy C-276	<2.5 (<0.1)	None	No
Inconel 625	<2.5 (<0.1)	None	No
AL 29-4	<2.5 (<0.1)	None	No
Hastelloy G	2.5 (0.1)	None	No
Incoloy 825	6.1 (0.24)	23	Yes
Inconel 690	13 (0.5)	90	Yes
304L SS	20 (0.80)	65	Yes
Inconel 671	28 (1.1)	20	Yes
316L SS	38 (1.5)	100	Yes
Carpenter 20 Cb-3	84 (3.3)	60	Yes
Inconel 600	102 (4.0)	65	Yes
Incoloy 800	330 (13)	12	Yes
E-Brite 26-1	460 (18)	16	Yes

[a]Tests performed with horizontal cylindrical specimen chamber.

Similar tests of 100-h duration were performed with some of the same alloys used in the previous tests and with type 317LM SS and EAS 2Si. The results, presented in Table 3.2, show that the latter two alloys performed somewhat better than the molybdenum-free iron- and nickel-based alloys, although pitting did occur. In addition, these data show that

Table 3.2. Corrosion rates (calculated from weight loss) and average pits depths (three deepest pits) for materials exposed 100 h to air containing 7.4×10^{-7} g/mL of iodine and 1.0×10^{-5} g/mL of H_2O at 25°C[a]

Material	Corrosion rate (μm/year)	Pit depth (μm)	Iodine deposition
Titanium	<2.5	None	No
Hastelloy C-276	<2.5	None	No
EAS 2 Si	152	15	Heavy[b]
317LM SS	197	38	Heavy[b]
316L SS	269	40	Heavy[b]
Incoloy 800	320	23	Heavy[b]
304L SS	324	139	Heavy[b]

[a] Tests performed in modified specimen chamber.
[b] Red-brown liquid phase.

corrosion of the other alloys (except titanium and Hastelloy C-276) was much greater than in the former tests, an effect that probably can be attributed to the use of the modified specimen chamber, which supplied a more uniform and generally greater iodine concentration to all specimens than did the original equipment.

During these tests it was noted that deposition of iodine-containing aqueous or solid phases occurred only on those specimens that underwent significant attack. This behavior was observed throughout the testing program except where much higher water contents were employed.

The influence of molybdenum concentration on weight loss and pitting of iron- and nickel-based alloys in iodine vapors at 25°C is given in Fig. 3.1. These data are average values taken from tests in which the iodine and water contents of the vapors were varied. It is apparent that >6% molybdenum in the alloy is required to impart immunity from attack in air containing iodine and water at 25°C.

3.1.2 Effect of exposure time

The influence of exposure time on the corrosion of selected candidate materials in air containing water and iodine at 25°C is displayed in Fig. 3.2 and Table 3.3. These data show that the depth of the pits on most alloys increased at a constant rate over the entire test period, as indicated by values close to one for the slopes of the curves plotted in Fig. 3.2. The cumulative corrosion rates calculated from weight-loss data for the susceptible materials increased over the initial 200 h and generally stabilized somewhat over the remaining 200 h (Table 3.3). The increase in weight loss with time over the initial 200 h of exposure was not unexpected because the surface area covered by the iodine-containing deposits increased during this period. Generally, after about 200 h, the surface was completely covered by the corrosive fluid. However, because of this, reproducibility from test to test was poor.

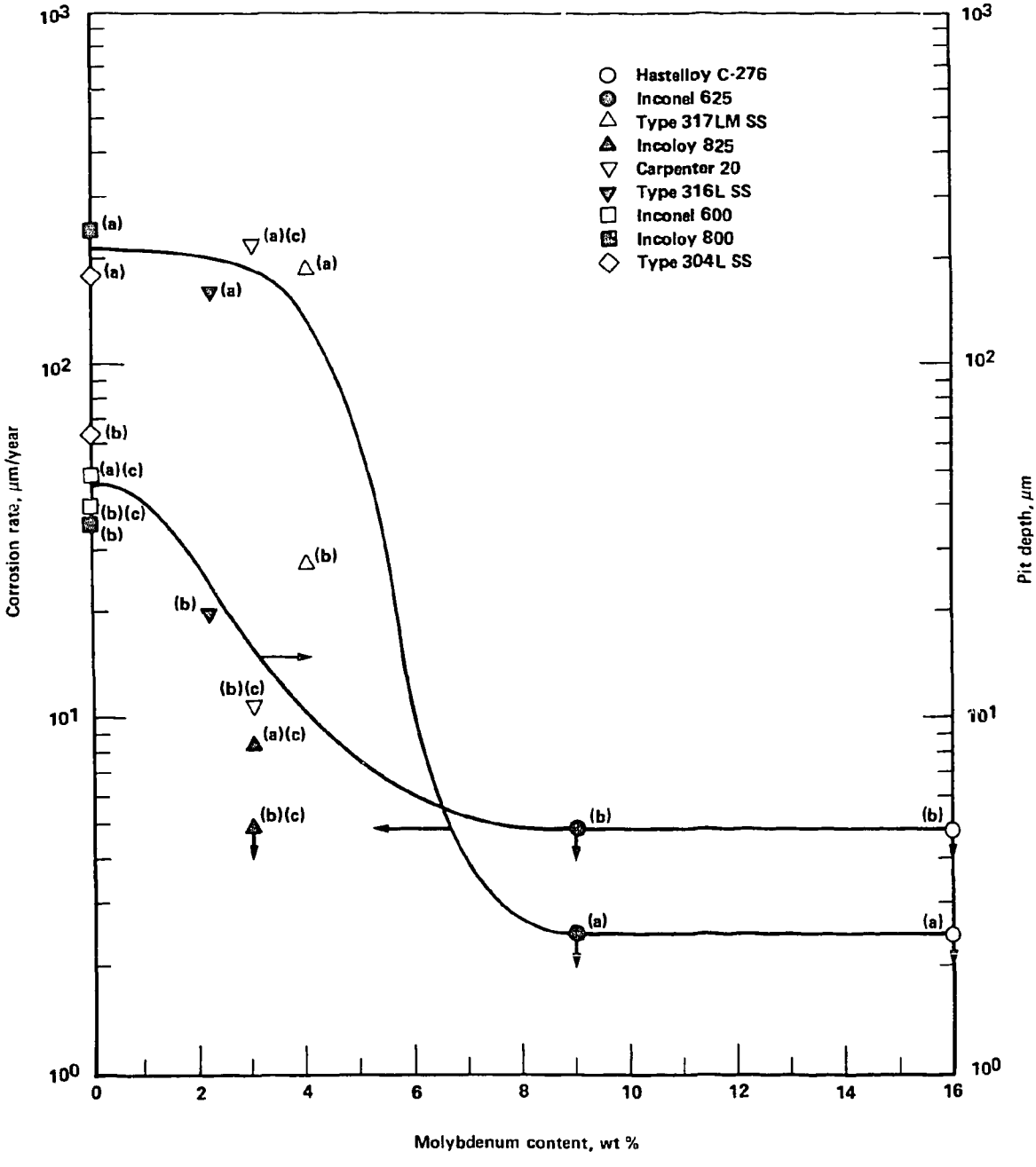

Fig. 3.1. Effect of molybdenum content of iron- and nickel-based alloys on pitting and weight loss in air containing 1.25×10^{-6} to 1.0×10^{-5} g/mL of H_2O and 9.3×10^{-8} to 7.4×10^{-7} g/mL of I_2 at 25°C; exposure time = 100 h. (Test performed with cylindrical specimen chamber.) (a) Corrosion rate, μm/y; (b) pit depth, μm; (c) data from single test.

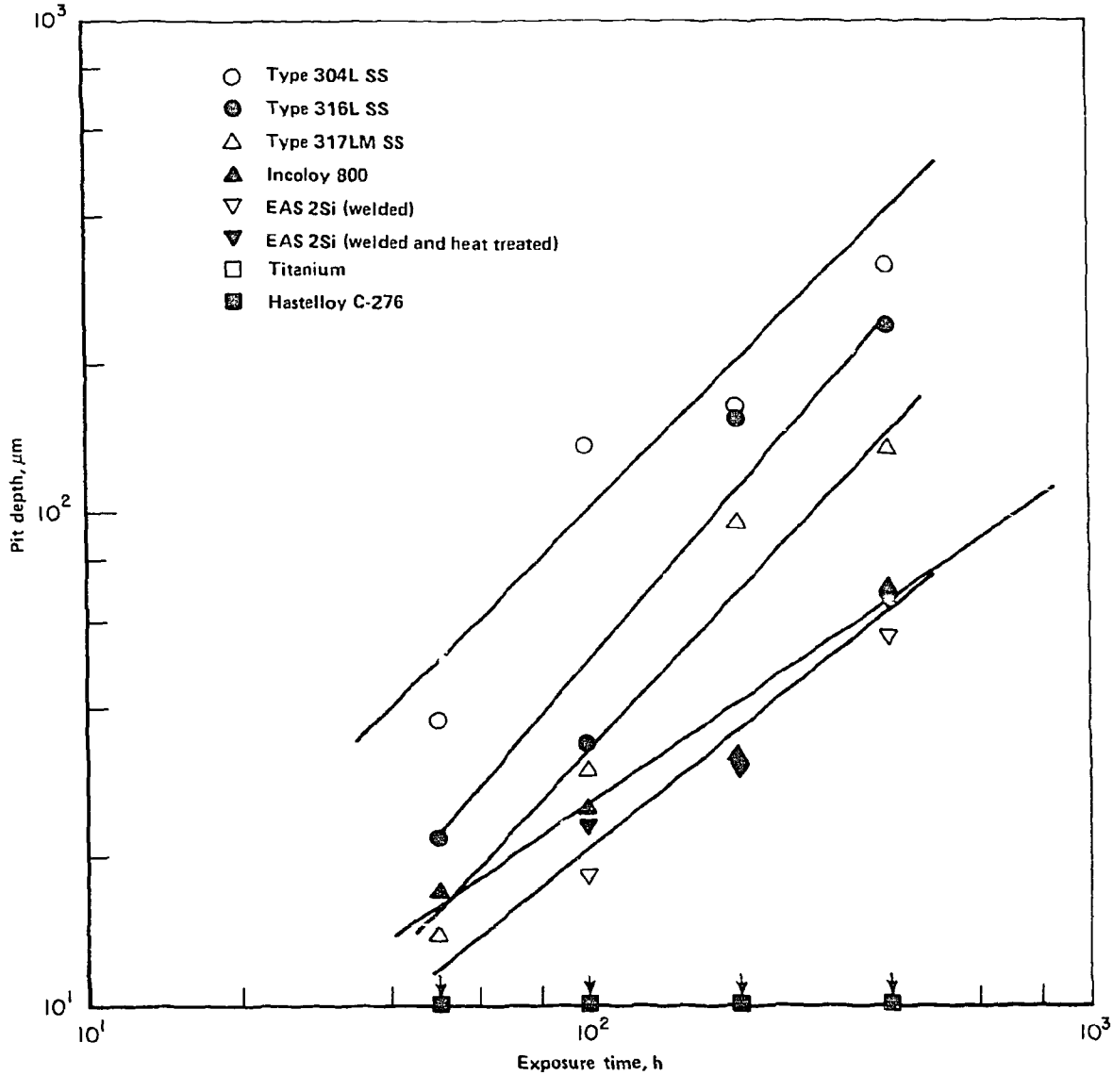

Fig. 3.2. Maximum pit depth (averaged for three deepest pits) as a function of exposure time for materials exposed to air containing 1.0×10^{-5} g/mL of H_2O and 7.4×10^{-7} g/mL of iodine at 25°C.

Table 3.3. Cumulative corrosion rates (calculated from weight loss) and maximum pit depths (three deepest pits) as a function of exposure time for materials exposed to air containing 1.0×10^{-5} g/mL of H_2O and 7.4×10^{-7} g/mL of iodine at 25°C

Material	Corrosion rate (μm/year)				Pit depth (μm)				α^a
	50 h	100 h	200 h	400 h	50 h	100 h	200 h	400 h	
Titanium	<2.5	<2.5	<2.5	<2.5	<5	<5	<5	<5	0
Hastelloy C-276	<2.5	<2.5	<2.5	<2.5	<5	<5	<5	<5	0
317LM SS	180	210	440	430	14	30	95	135	1.1
Incoloy 800	310	420	750	820	17	25	32	70	0.7
316L SS	360	460	650	730	22	34	155	240	1.2
304L SS	295	330	710	660	38	135	165	315	1.0
EAS 2 Si (welded)	210	210	420	410	5.0	23	30	65	0.8
EAS 2 Si (welded and heat treated)	310	250	410	420	5.0	18	30	55	0.8

[a]Slopes of curves found in Fig. 3.2.

3.1.3 Effect of temperature

The influence of temperature on attack of selected materials was studied in air containing a fixed concentration of water and iodine. Results, presented in Table 3.4, indicate that the number of alloys on which attack occurred decreased with increasing temperature at a constant water concentration and that no attack was observed on any of the materials at 70°C. However, data to be presented later in the report show that attack can be quite severe if the relative humidity is held constant as the temperature is increased.

3.1.4 Effect of vapor composition

The influence of the gas composition on the rate of attack of the candidate alloys was examined by varying the H_2O, iodine, and NO_2 concentrations. In addition, the carrier gas was changed from air to N_2 in one test to examine its influence on the severity of attack. A comparison of the results of the latter test (Table 3.5) with the results of similar tests performed in air (Table 3.1) suggests that the attack, in most cases, was somewhat greater in nitrogen than in air. However, considering that all tests were conducted in the horizontal chamber and that reproducibility was generally poor, it was concluded that there was no major difference between the two sets of results.

Effect of water content. The influence of the water content of air containing iodine on the corrosion of materials was studied at 25°C. The results, given in Table 3.6, indicate that the severity of attack increased with increasing water content. However, studies performed

Table 3.4. Effect of temperature on corrosion rates (calculated from weight loss) and on pit depths (calculated for three deepest pits) for alloys exposed to air containing 7.4×10^{-7} g/mL of iodine and 1.0×10^{-5} g/mL of H_2O during 175-h exposure[a,b]

Material	Corrosion rate (μm/year)					Pit depth (μm)				
	25°C	40°C	50°C	60°C	70°C	25°C	40°C	50°C	60°C	70°C
Titanium	<2.5	<2.5	<2.5	<2.5	<2.5	<5	<5	<5	<5	<5
Zirconium	<2.5	<2.5	<2.5	<2.5	<2.5	<5	<5	<5	<5	<5
Hastelloy C-276	<2.5	<2.5	<2.5	<2.5	<2.5	<5	<5	<5	<5	<5
Inconel 625	<2.5	<2.5	<2.5	<2.5	<2.5	<5	<5	<5	<5	<5
Incoloy 825	6.1[c]		3.4	<2.5	<2.5	23[c]		15	<5	<5
Carpenter 20 Cb-3	84[c]		7.8	4.2	<2.5	60[c]		7	<5	<5
316L SS	270	320[d]	90	5.2	<2.5	200	35[d]	<5	<5	<5
304L SS	250	420[d]	170	260	<2.5	215	270[d]	10	15	<5

[a] Concentrations are at 25°C; these decreased slightly at the higher temperature.
[b] Cylindrical specimen chamber.
[c] 400-h exposure.
[d] 100-h exposure.

Table 3.5. Corrosion rates (calculated from weight loss) and pit depths (averaged for three deepest pits) for duplicate tests of materials exposed for 200 h to N_2 containing 7.4×10^{-7} g/mL of iodine and 1.0×10^{-5} g/mL of H_2O at 25°C[a]

Material	Corrosion rate (μm/year)	Pit depth (μm)	Iodine deposition
Titanium	<2.5	<5	No
Zirconium	<2.5	<5	No
Inconel 625	27	<5	Yes[b]
Hastelloy C-276	30	<5	Yes[b]
Inconel 600	46	35	Yes[b]
304L SS	78	20	Yes[b]
Incoloy 800	155	30	Yes[b]
316L SS	175	<5	Yes[b]
Incoloy 825	230	<5	Yes[b]
Carpenter 20	270	<5	Yes[b]

[a] Horizontal cylindrical specimen chamber.
[b] Green liquid-phase deposit.

Table 3.6. Effect of water content [relative humidity (RH)] on corrosion rate (calculated from weight loss) and on maximum pit depth (averaged for three deepest pits) of materials exposed to air containing 7.4×10^{-7} g/mL of iodine for 100 h at 25°C[a]

Material	Corrosion rate (μm/year)						Pit depth (μm)					
	<0.5% RH	2.2% RH	5.4% RH	11% RH	22% RH	44% RH	<0.5% RH	2.2% RH	5.4% RH	11% RH	22% RH	44% RH
Titanium	<2.5	<2.5	<2.5	<2.5	<2.5	<2.5	<5	<5	<5	<5	<5	<5
Zirconium	<2.5	<2.5	<2.5			<2.5	<5	<5	<5			<5
Hastelloy C-276	<2.5	<2.5	<2.5			<2.5	<5	<5	<5			<5
Inconel 625	5.2	<2.5	<2.5	<2.5	<2.5	<2.5	<5	<5	<5	<5	<5	<5
Incoloy 825	4.9	2.6	<2.5	<2.5	14	6.1	<5	<5	<5	<5	<5	23
Inconel 600	3.4	4.0	49			102	<5	<5	38			65
Carpenter 20 Cb-3	7.2	3.1	185			270	<5	<5	11			<5
316L SS	7.1	7.9	220			269	<5	<5	<5			40
304L SS	6.7	6.3	355		650	324[b]	<5	<5	60		55	139[b]

[a]Cylindrical specimen chamber.
[b]Test performed in modified desiccator.

at 40°C indicate that the rate of attack decreased at very high humidities (see Table 3.7) or under reflux conditions (see Sect. 3.3). At all water contents studied, significant attack occurred only on those alloys on which iodine deposition occurred. However, the morphology of the deposits varied with the water content of the air. At low humidity levels, the morphology of the iodine-containing deposits was identical to that of the deposits found in the elevated temperature tests, viz., solid-phase black deposits covering the entire surfaces of the specimens. The morphology of the deposits on type 304L SS tested at 25°C changed from a uniform, black, solid deposit to a solution at water contents in the vapor ranging between 2.5×10^{-6} g/mL and 5.0×10^{-6} g/mL. The attack was generally uniform under low humidity conditions with considerably less severe pitting than was observed under higher humidity conditions. It was also observed that a liquid phase formed on alloys previously exposed under low humidity conditions (on which the black solid-phase deposits were present) when the specimens were later exposed to humidified air. Rapid pitting then ensued.

Table 3.7. Corrosion rates (calculated from weight loss) and maximum pit depths (averaged for three deepest pits) as a function of NO_2 and H_2O concentration for type 304L SS specimens exposed for 100 h to air containing 5.7×10^{-7} g/mL of iodine at 40°C

H_2O concentration (g/mL)	Relative humidity (%)	NO_2 concentration (g/mL)	Corrosion rate (μm/year)	Maximum pit depth (μm)
3.5×10^{-5}	68		12.5	None
1.75×10^{-5}	34		680	45
1.75×10^{-5}	34	6.8×10^{-6}	23	15

Effect of iodine concentration. The influence of the iodine concentration of humidified air on the corrosion of selected candidate materials was studied at 25 and 40°C. Results given in Figs. 3.3 through 3.6 show that, in most instances, the weight loss of the specimens and the maximum depth of pitting increased with the increasing iodine concentration of the vapors. However, significant attack occurred on the susceptible materials at the lowest iodine concentration evaluated. Maximum pit depths were somewhat less dependent on iodine content at the higher temperature. Rates of weight loss were comparable at the two test temperatures, but pitting rates were slightly greater at 40 than at 25°C.

Effect of NO_2. The influence of NO_2 concentration on the corrosion of type 304L SS was evaluated in air containing 1.0×10^{-5} g/mL of H_2O and 5.9×10^{-7} g/mL of I_2 at 25°C. Results, given in Fig. 3.7, show that attack was inhibited at NO_2 concentrations greater than 8×10^{-6} g/mL, which corresponds to a mole ratio of water to NO_2 of 0.3.

Similar tests were performed on type 304L SS in air containing iodine and water at 40°C. Results, given in Table 3.7, show that NO_2 also was effective in inhibiting attack at 40°C.

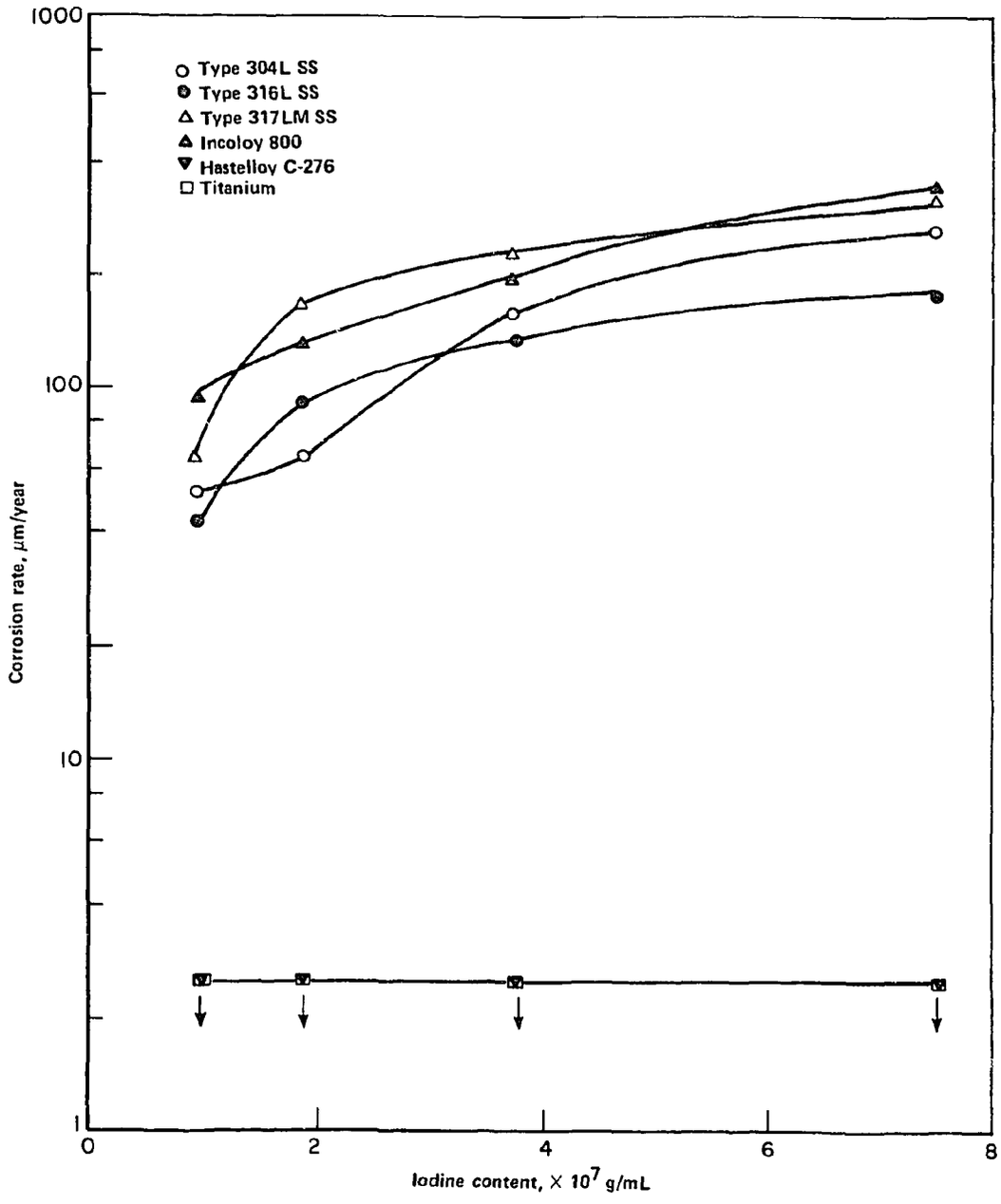

Fig. 3.3. Effect of iodine concentration in gas streams on the corrosion rate (calculated from weight loss) for selected materials exposed 100 h to air containing 1.0×10^{-5} g/mL of H_2O at 25°C; total flow rate = 80 mL/min. (Test performed with horizontal cylindrical specimen chamber.)

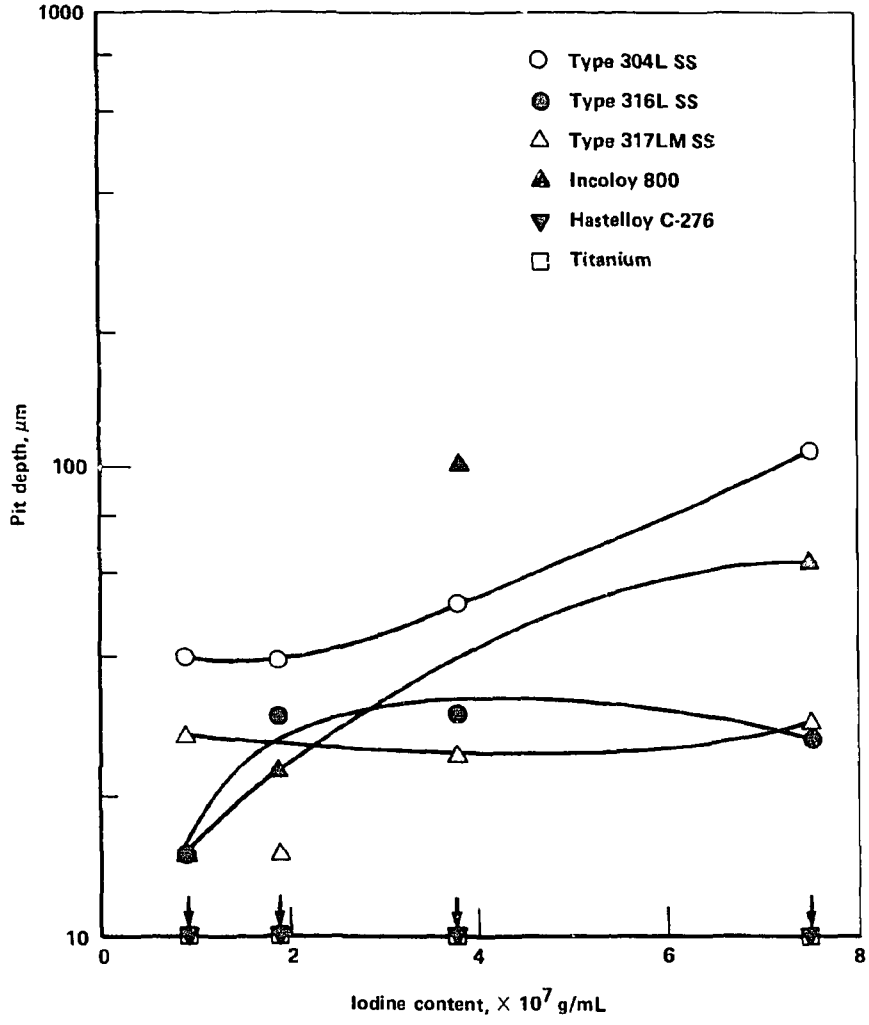

Fig. 3.4. Effect of iodine concentration in gas streams on maximum pit depth (average for three deepest pits) for selected materials exposed 100 h to air containing 1.0×10^{-5} g/mL H_2O at 25°C; total flow rate = 80 mL/min.

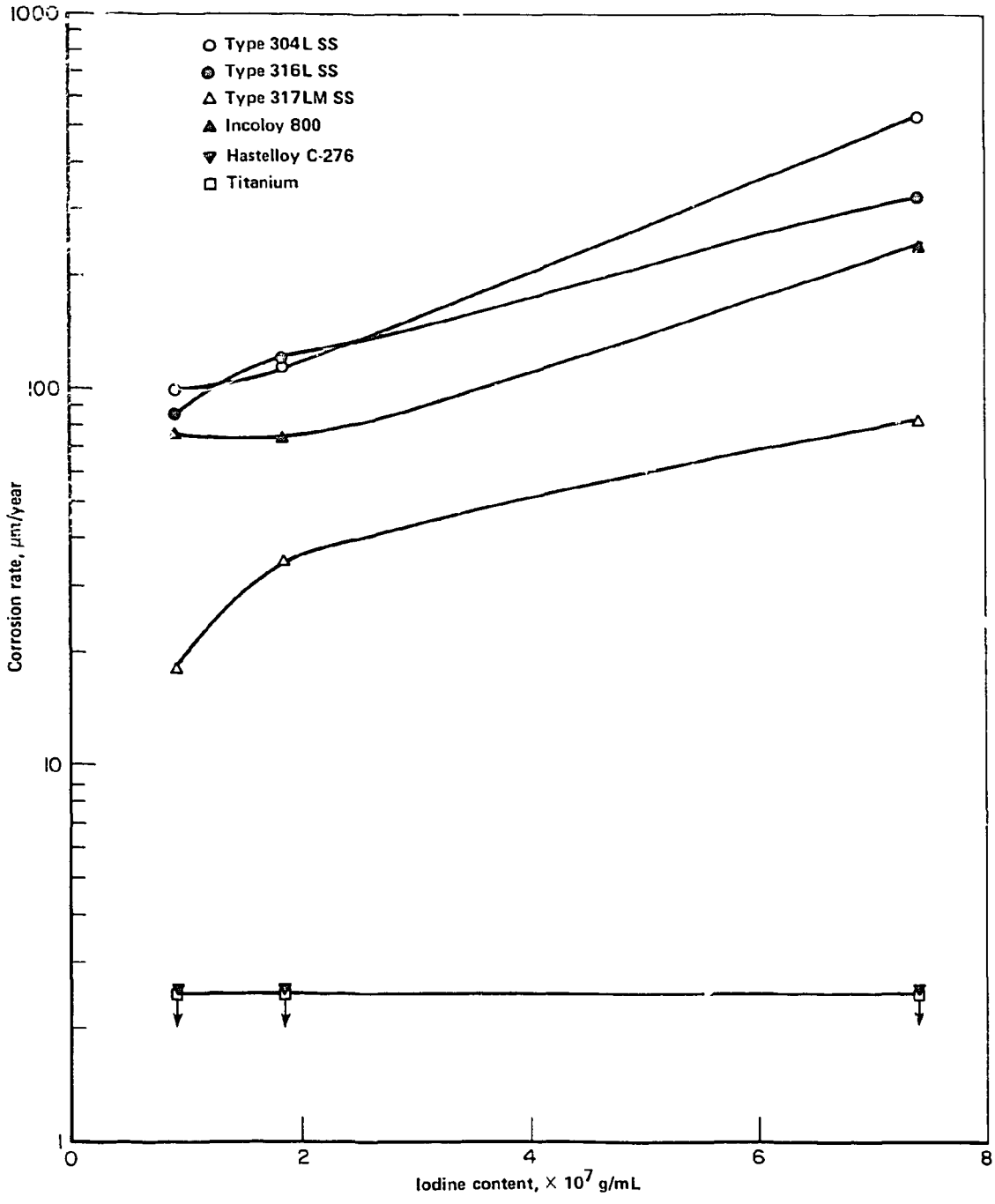

Fig. 3.5. Effect of iodine concentration in gas streams on the corrosion rate (calculated from weight loss) for selected materials exposed 100 h to air containing 1.0×10^{-5} g/mL of H_2O at 40°C; total flow rate = 80 mL/min.

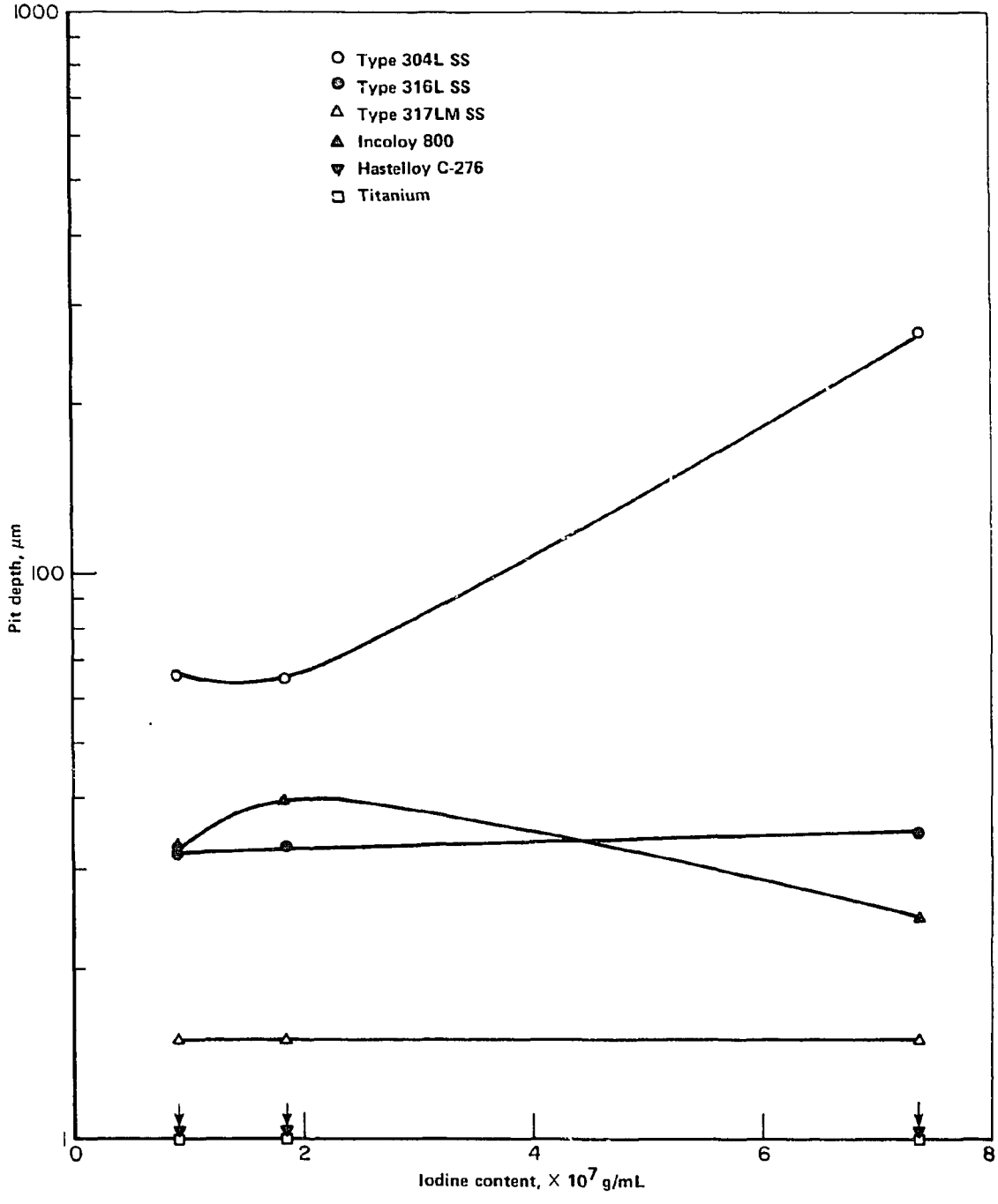

Fig. 3.6. Effect of iodine concentration in gas streams on maximum pit depth (averaged for three deepest pits) for selected materials exposed 100 h to air containing 1.0×10^{-5} g/mL of H_2O at 40°C; total flow rate = 80 mL/min. (Test performed with cylindrical specimen chamber.

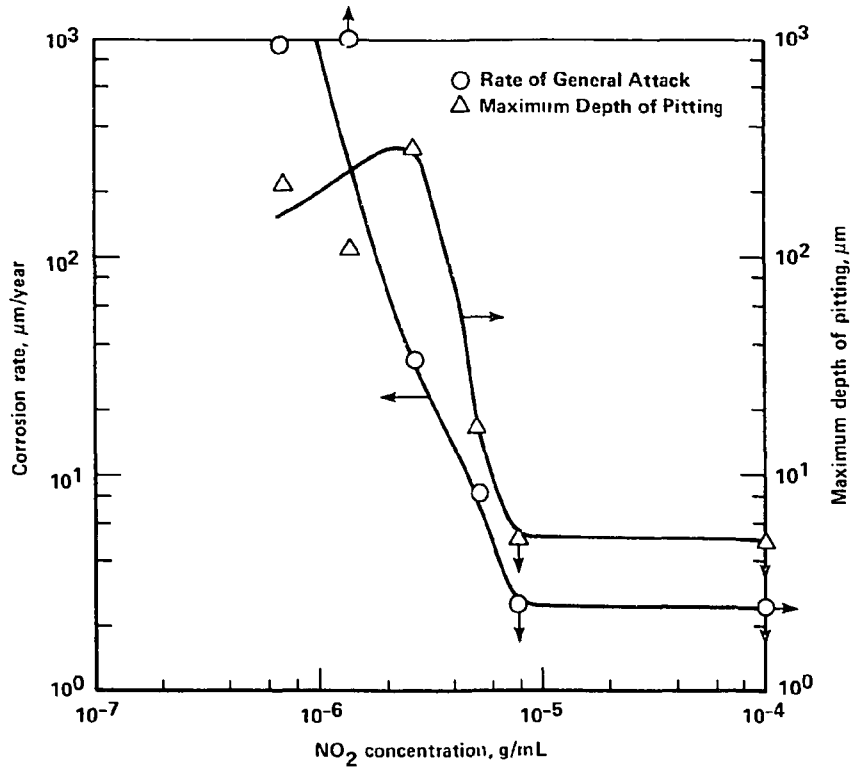

Fig. 3.7. Effect of NO_2 concentration on the maximum depth of pitting (calculated from three deepest pits) and the corrosion rate (calculated from weight loss) for duplicate specimens of type 304L SS exposed for 100 h at 25°C to air containing 1.05×10^{-5} g/mL of H_2O and 5.9×10^{-7} g/mL of I_2.

3.1.5 Deposit analyses

Specimens of Armco Iron and Nickel 201 were exposed to air containing 1.0×10^{-5} g/mL of H_2O and 7.4×10^{-7} g/mL of iodine for 100 h at 40°C. Black solid-phase deposits formed on the surfaces of both specimens, and significant attack occurred beneath the deposits. X-ray diffraction patterns were obtained from the deposits. Results given in Table 3.8 indicate no evidence of elemental iodine on the specimen surfaces, but both NiI_2 and FeI_2 were probably present. These compounds are deliquescent, which accounts for the liquid phases that formed in humid air.

Table 3.8. X-ray diffraction analyses of deposits formed on Armco Iron and Nickel 201 during exposure for 100 h at 40°C to air containing 1.0×10^{-5} g/mL of H_2O and 7.4×10^{-7} g/mL of iodine

Sample	Compound	PDF number	Pattern strength
Armco Iron	$FeCl_2 \cdot 2H_2O$[a]	25-1040	Strong
	FeO(OH) (Akaganeite)	13-157	Very weak
Nickel 201	NiI_2	20-785	Medium
	$NiCl_2 \cdot 2H_2O$[b]	1-1143	Weak
	Unknown[c]		Strong

[a]This phase is believed to be $FeI_2 \cdot 2H_2O$, which is not contained in the powder diffraction file.

[b]This phase is believed to be $NiI_2 \cdot 2H_2O$, which is not contained in the powder diffraction file.

[c]This is the strongest line in the pattern and is not attributable to an identified phase.

3.2 Tests in Apparatus B

In tests with Apparatus B, the influence of the concentration of HNO_3 on the corrosion rate of type 304L SS specimens located in the vapor phase above the boiling solution was evaluated in vapors containing 7.4×10^{-7} g/mL iodine. The specimens were held at 25°C. Results given in Fig. 3.8 show that the corrosion rate of the specimens decreased with increasing concentration of HNO_3 and that no attack was observed at concentrations greater than 12 *M*.

3.3 Tests in Apparatus C

The influence of temperature on the corrosion of candidate materials on which iodine crystals were placed was evaluated in tests in which the specimens were suspended horizontally above 8 *M* HNO_3 for 100 h. Results presented in Table 3.9 show that attack of the

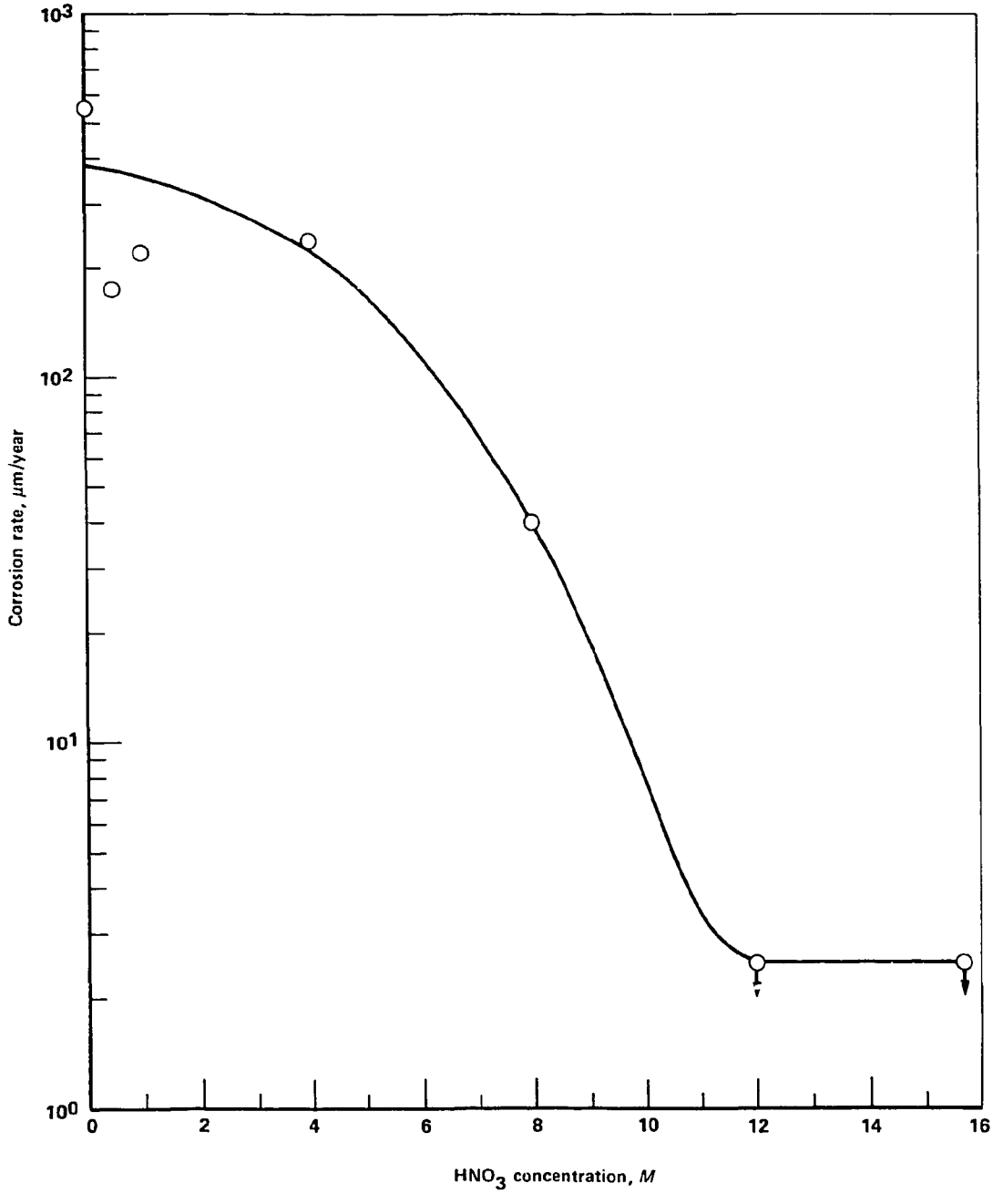

Fig. 3.8. The influence of HNO_3 concentration on corrosion rates (calculated from weight loss) for duplicate type 304L SS specimens exposed for 100 h above boiling HNO_3 solutions in vapors containing approximately 7.4 X 10^{-7} g/mL of iodine.

Table 3.9. Effect of temperature on corrosion rates (calculated from weight loss) and maximum pit depths (averaged for three deepest pits) for candidate materials exposed 100 h above 8 *M* HNO_3 with iodine crystals on the specimen surfaces

Material	Corrosion rate (μm/year)					Maximum pit depth (μm)				
	25°C	35°C	50°C	65°C	85°C	25°C	35°C	50°C	65°C	85°C
Titanium	7.6	3.3	<2.5	16	8.1	<5	<5	<5	<5	<5
Zirconium	<2.5	<2.5	10	190	<2.5	<5	<5	<5	<5	<5
Hastelloy C-276	4.1	8.1	33	16	41	<5	<5	<5	<5	<5
Hastelloy G	<2.5	3.6	<2.5	4.0	8.1	<5	<5	<5	<5	<5
Inconel 625	<2.5	3.3	9.0	9.0	7.9	<5	<5	<5	<5	<5
AL 29-4	<2.5	9.4	19	85	9.4	<5	<5	<5	<5	<5
E-Brite 26-1	9.4	135	700	690	21	<5	<5	240	25	70
Incoloy 825	5.6	43	740	36	62	<5	<5	120	15	65
Carpenter 20 Cb-3	1,200	5,400	2,050	3,200	175	570	130	470	125	45
Inconel 690	1,600	4,350	4,900	3,550	2,700	15	80	290	60	150
Inconel 671	130	3,300	1,800	1,400	1,200	<5	15	80	65	30
Inconel 600	4,000	5,600	7,700	12,600	23,000	360	195	160	P[a]	P[a]
Incoloy 800	3,300	6,800	4,350	2,300	2,100	245	60	270	50	165
316L SS	2,100	3,000	4,000	3,100	1,200	360	240	375	200	375
304L SS	1,500	3,300	2,700	3,050	1,300	175	515	310	750	210

[a]Perforated (1575 μm).

candidate materials generally increased with increasing temperature. As was found in the previously reported studies, titanium, zirconium, and the iron- and nickel-based alloys containing significant amounts of molybdenum were very resistant to attack, whereas those alloys containing less than 6% molybdenum were corroded (see Fig. 3.9).

The influence of the concentration of boiling HNO_3 on the corrosion rate of type 304L SS was evaluated in supersaturated iodine vapors. In an initial series of tests the condenser was fabricated of type 304L SS and functioned as the test specimen. In all tests iodine crystals rapidly formed on the inside of the tubes. No attack occurred in the vapors above 12 and 15.7 *M* solutions, whereas localized attack occurred beneath the iodine crystals in vapor exposure above an 8 *M* HNO_3 solution. The test in 8 *M* HNO_3 was repeated, and an additional test was run in 4 *M* HNO_3. In contrast to the previously reported results, no attack was observed in either test, indicating that parameters other than HNO_3 concentration were influencing the rate of attack. One likely candidate was the reflux rate of the system; the condensate may dilute any deleterious aqueous phase that forms under or around the iodine crystals. Dilution is possible in Apparatus C because of the proximity of the specimen to the boiling solution, whereas it is relatively unlikely in Apparatus B. However, the beneficial effects of the condensate may not extend to restricted geometries such as crevices.

Tests were carried out to evaluate the influence of reflux rate, crevices, NO_2 and HNO_3 concentration, and preexposure to HNO_3 on attack of type 304L SS in supersaturated iodine vapors. In the preexposure tests the specimens were exposed above the boiling 4

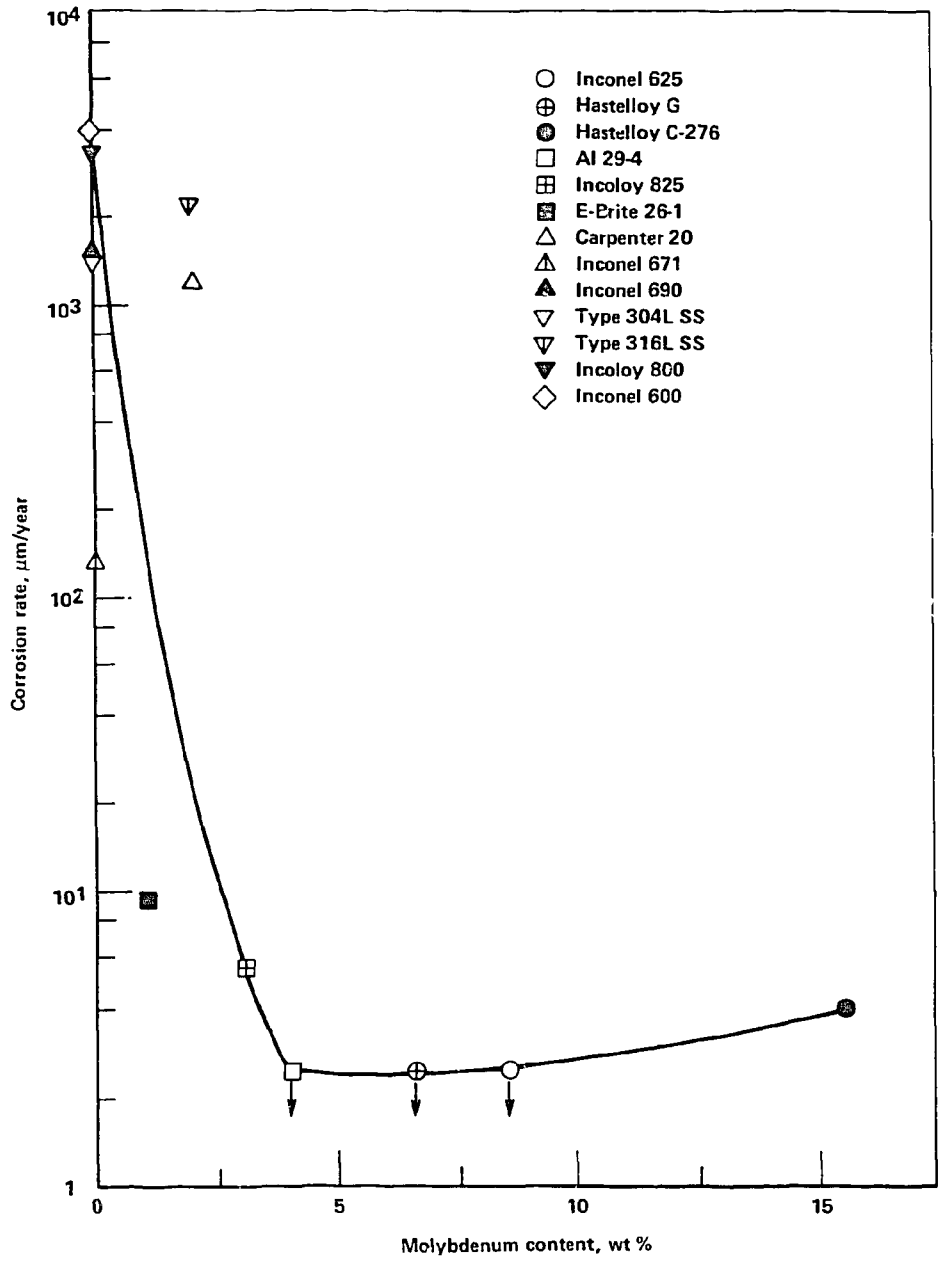

Fig. 3.9. The effect of molybdenum content of iron- and nickel-based alloys on corrosion in vapors above 8 *M* HNO_3 at 25°C with iodine crystals on specimen surfaces.

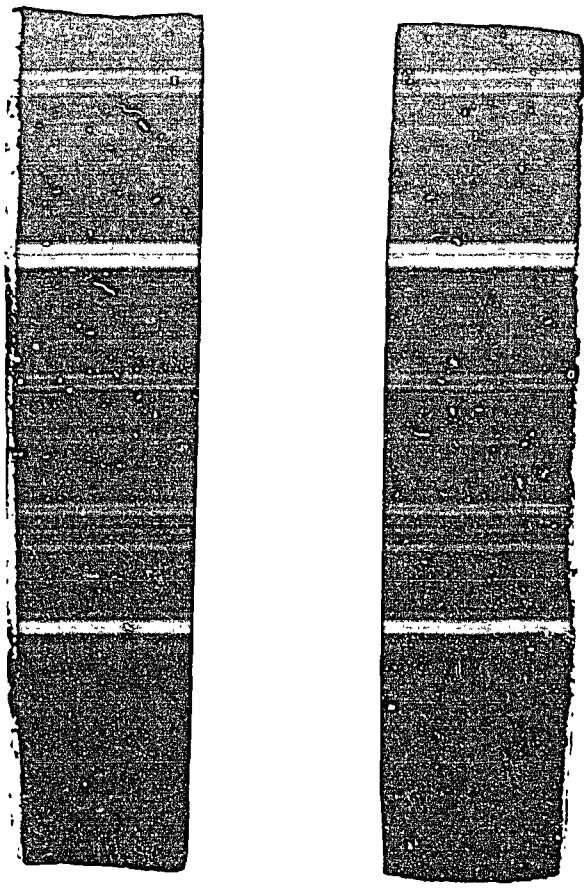

2X 2KO74

Fig. 3.10. Low-power optical photograph of type 304L SS specimens following 100 h of exposure above 4 *M* HNO_3 to which 10 g of iodine crystals was added. Left – boldly exposed face; right – crevice face.

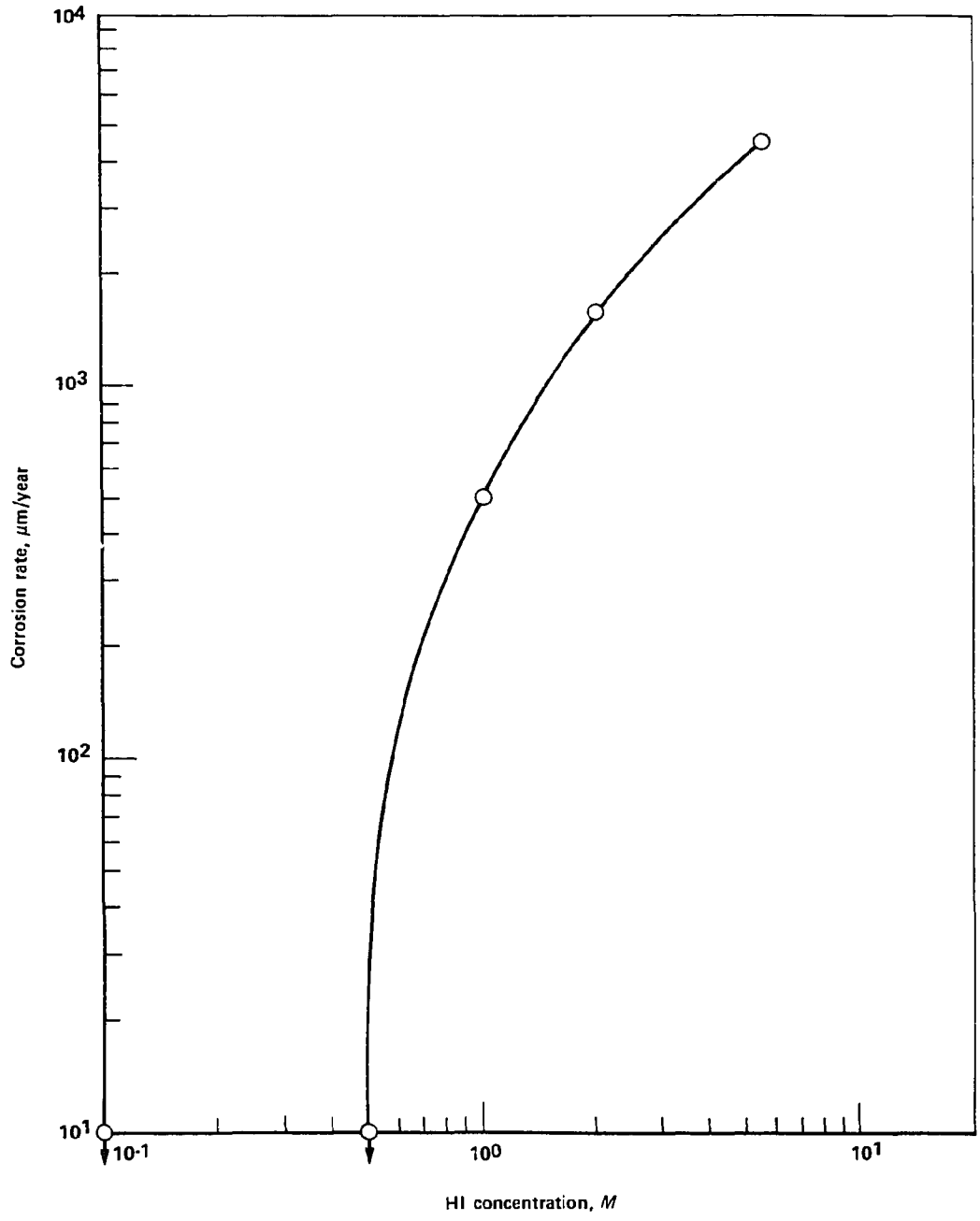

Fig. 3.11. Effect of HI concentration on the corrosion rate (calculated from weight loss) for type 304L SS exposed 120 h at 25°C under aerated conditions with iodine crystals on the specimen surfaces.

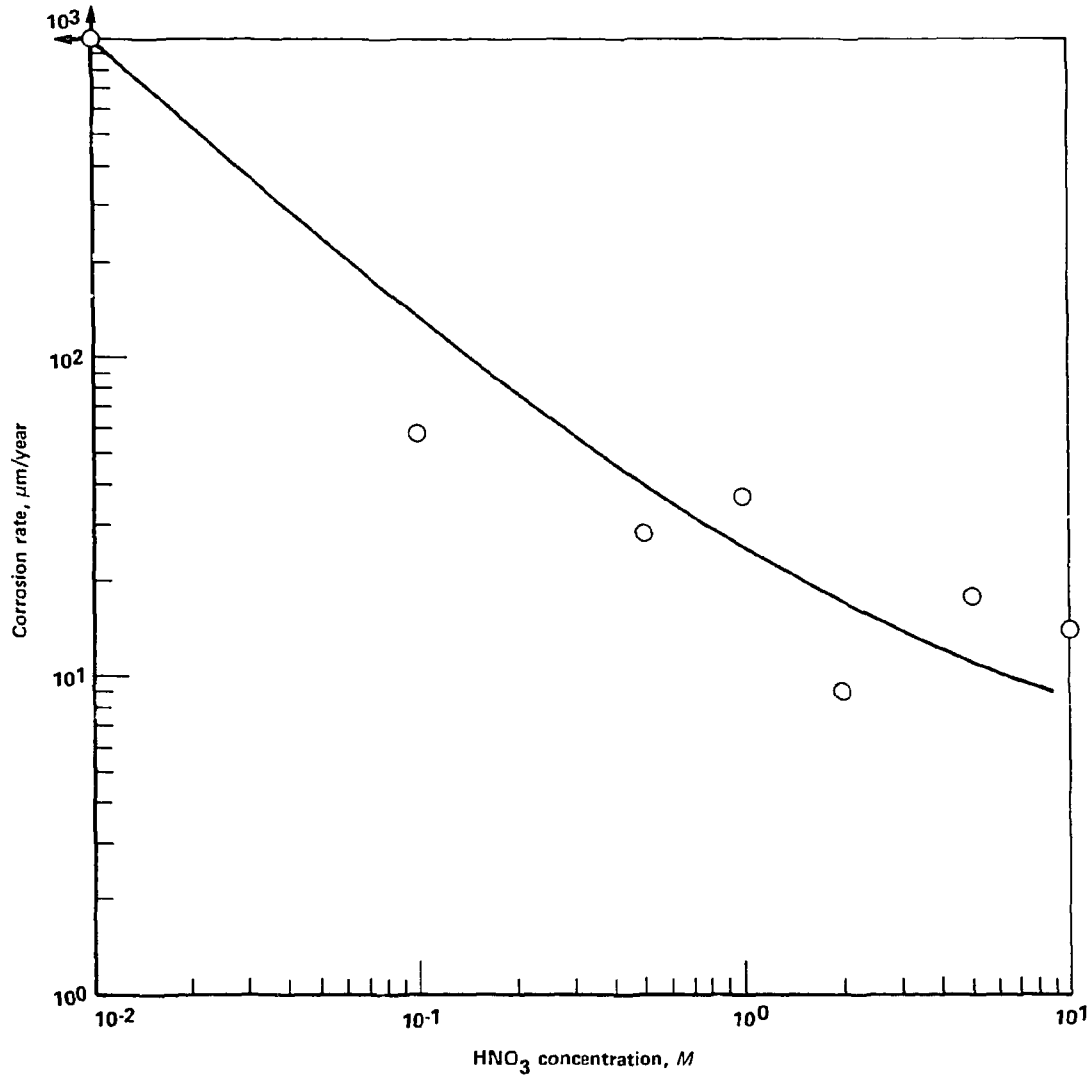

Fig. 3.12. Effect of HNO_3 concentration on the corrosion rate (calculated from weight loss) for type 304L SS exposed 50 h at 25°C to 2 *M* HI under aerated conditions with iodine crystals on the specimen surfaces.

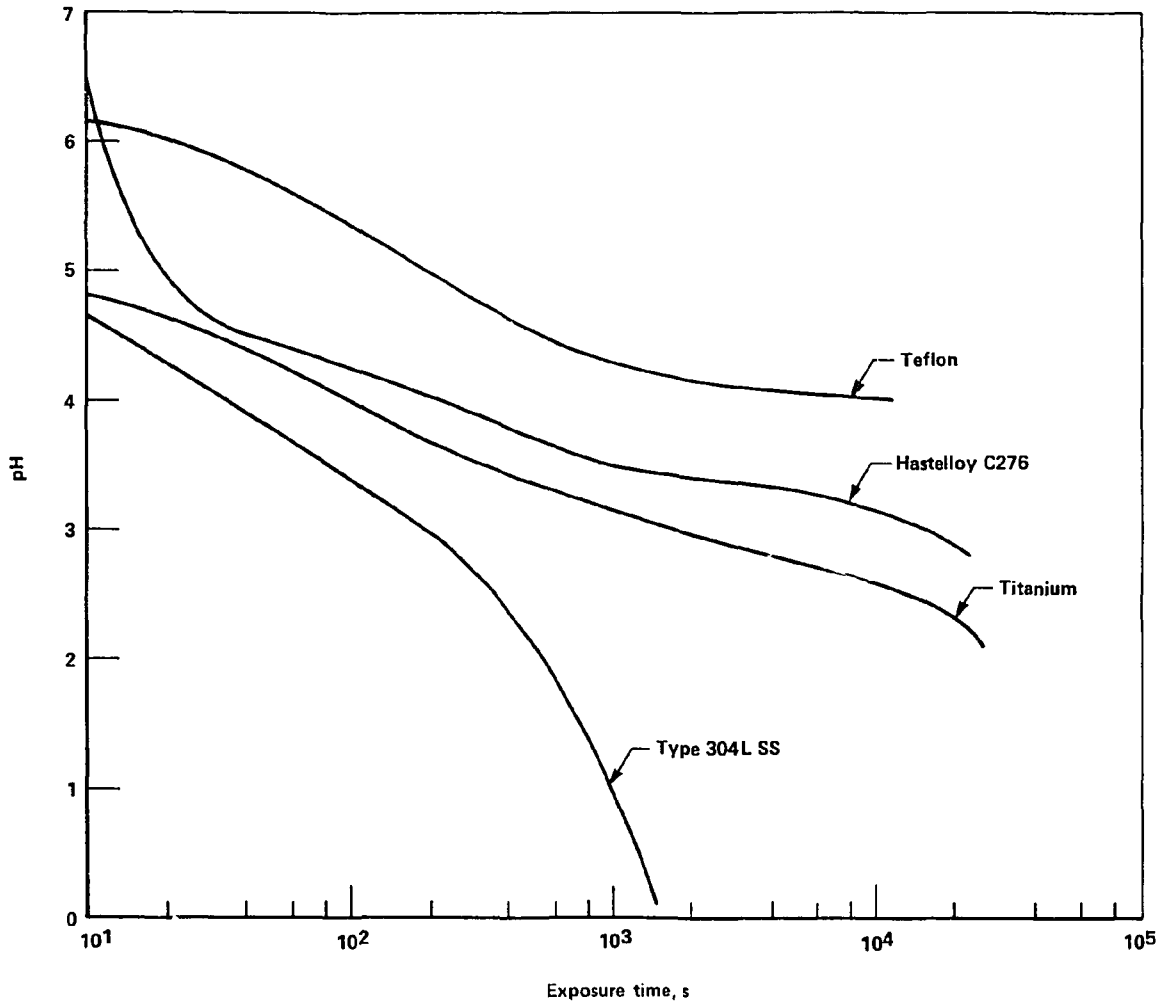

Fig. 3.13. The pH as a function of exposure time for distilled water in contact with iodine crystals on various materials at 25°C under naturally aerated conditions.

M HNO_3 for 4 h prior to exposure to the iodine. The results are summarized in Table 3.10. These data suggest that attack of boldly exposed surfaces is inhibited by condensate reflux even at temperatures below boiling. However, the beneficial effects do not extend to the crevice regions, where severe attack was observed. A typical example is shown in Fig. 3.10. Preexposure to HNO_3 also appears to have little effect on the crevice attack. On the other hand, HNO_3 at high concentrations and the presence of NO_2 were partially effective in minimizing crevice attack, but the beneficial effects were not nearly so great as those observed on the free surfaces.

Table 3.10. Results of 100-h tests on type 304L SS specimens located above HNO_3 in which 10 g of iodine crystals was added

Test number	HNO_3 concentration (*M*)	Temperature (°C)	Crevices present	NO_2 concentration (g/mL)	HNO_3 preexposure	Corrosion rate (μm/year)	Crevice attack	Maximum depth of attack (μm)
A	4	90	No		No	<2.5		<5
B	4	Boiling	No		No	4.0		<5
C	4	Boiling	Yes		No	390	Yes	145
D	4	Boiling	Yes		Yes	1100	Yes	280
E	4	Boiling	Yes	1×10^{-5}	No	240	Yes	[a]
F	15.7	Boiling	Yes		No	4.0	Yes	127
G[b]	15.7	Boiling	Yes		No	<2.5	No	<5

[a] General etching in crevice region.
[b] Repeat of test F.

3.4 Results of Other Tests

Exposure tests were carried out on type 304L SS at 25°C in HI of various concentrations and in 2 *M* HI containing HNO_3. All tests were under naturally aerated conditions, and 1 g of iodine crystals was placed on the specimen surfaces at the initiation of the tests. Results presented in Figs. 3.11 and 3.12 indicate that the rate of attack was a strong function of HI concentration and that HNO_3 inhibited corrosion. The attack was uniform.

In other tests the potential of Hastelloy C-276, commercial-grade titanium, and type 304L SS was measured relative to the saturated calomel electrode (SCE) as a function of exposure time in the presence of iodine crystals and distilled water under naturally aerated conditions at 25°C. In the absence of iodine, the corrosion potentials of Hastelloy C-276 and type 304L SS rapidly stabilized at values slightly negative to the SCE; that of titanium gradually increased. The potentials of all of the materials tested increased rapidly upon the addition of elemental iodine and stabilized at noble values for the duration of the tests. Potential values are given in Table 3.11.

The pH of the solutions on the above alloys and on Teflon was also measured. The results (given in Fig. 3.13) show that the pH of the solution on the type 304L SS dropped rapidly with time, achieving values of less than 0.1 within 1 h. The pH of the solutions on titanium and Hastelloy C-276 dropped more rapidly than on Teflon but never fell below 2.

Table 3.11. The corrosion potentials of three materials under a drop of distilled water before and after placing iodine crystals in the water

Material	Corrosion potential,[a] V	
	Before	After
Titanium	+0.105	+0.420
Hastelloy C-276	−0.165	+0.450
304L SS	−0.145	+0.265

[a]Saturated calomel electrode.

The pH as a function of exposure time was also measured for aerated distilled water in the presence of selected combinations of nickel, iron, chromium, nickelous sulfate, ferrous sulfate, potassium iodine, and elemental iodine. Tests with iron, chromium, and nickel were performed on Armco Iron, electrolytic chromium, and Nickel 201 surfaces, respectively, whereas all other tests were performed on Teflon. The results (given in Fig. 3.14) show that the most pronounced drop in pH occurred on the nickel and iron surfaces on which iodine crystals were placed. A relatively lower drop in pH occurred on the chromium surfaces in the presence of iodine and on the Teflon surfaces in the presence of ferrous ion and iodine. The smallest drop in pH occurred in the presence of nickelous ion and iodine.

The effect of aeration on the pH of aqueous iodine solutions on Armco Iron and Nickel 201 surfaces was also measured. Aerated tests were performed in laboratory air, and deaerated tests were performed in a glove bag purged with nitrogen. The results, given in Fig. 3.15, show that the degree of aeration had little effect on the pH of the solutions.

4. DISCUSSION

The results of the experimental program indicate that the commonly used stainless steels, types 304L and 316L, undergo severe pitting attack in air that contains elemental iodine and water vapors. On the other hand, titanium, zirconium, and the iron- and nickel-based alloys containing a minimum of 6% molybdenum were much more resistant to attack. Substitution of N_2 for air did not have a significant effect on rates of attack. In the susceptible materials, the rates at which pits deepened were nearly constant over a 400-h exposure. Rates of attack decreased with increasing temperature when the iodine and water concentrations of air were held constant, whereas the opposite was true in tests performed at nearly constant relative humidities. Similarly, rates of attack of susceptible alloys on which iodine crystals were placed increased with increasing temperature in tests performed on specimens located above 8 *M* HNO_3.

The corrosion of susceptible candidate materials increased with the increasing water content of the gas stream at 25°C and at elevated temperatures except where very high humidity conditions were encountered. The exposure of susceptible materials to iodine vapors containing very low concentrations of water produced a black solid on the surfaces

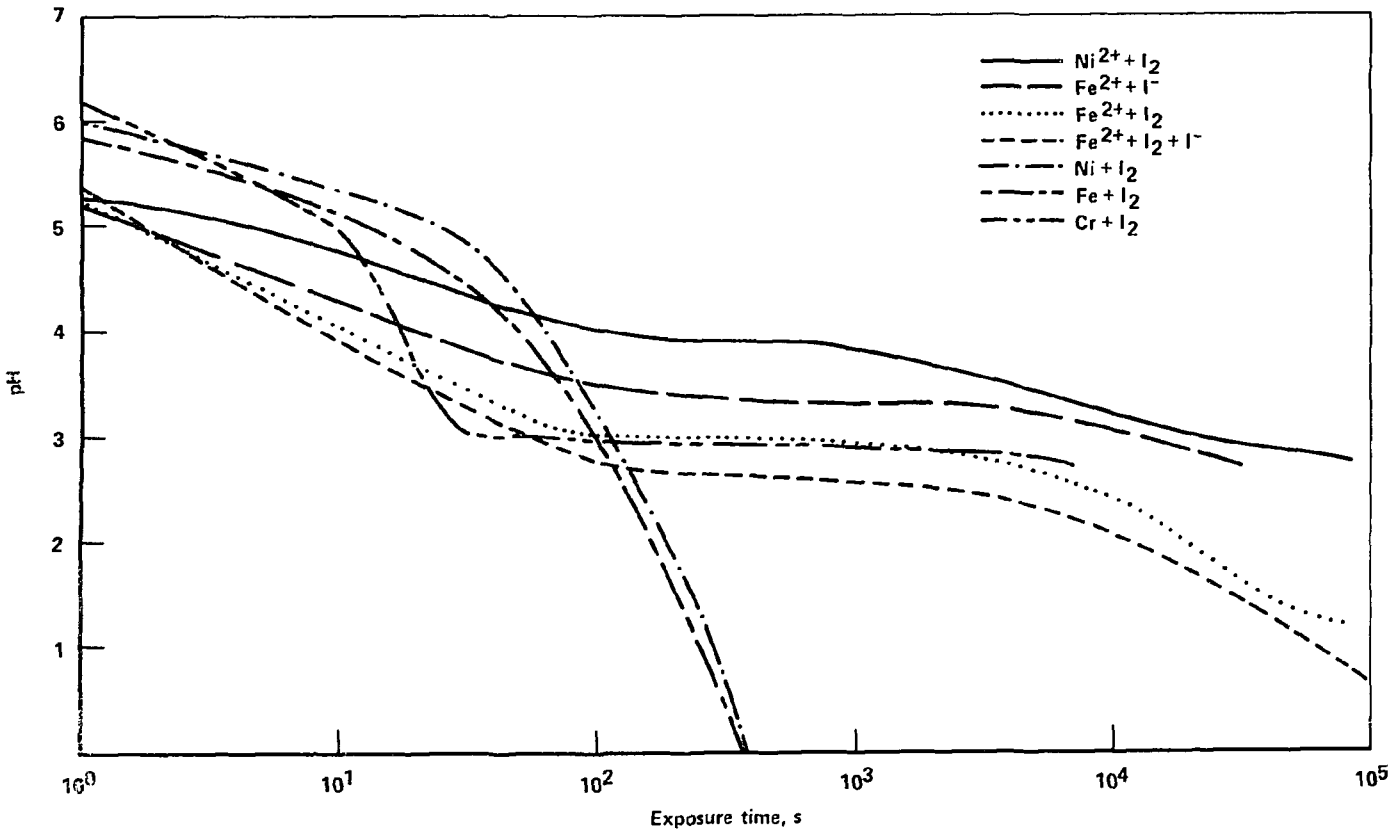

Fig. 3.14. The pH as a function of exposure time for distilled water (0.1 mL) in contact with elemental iodine and various metals and salts.

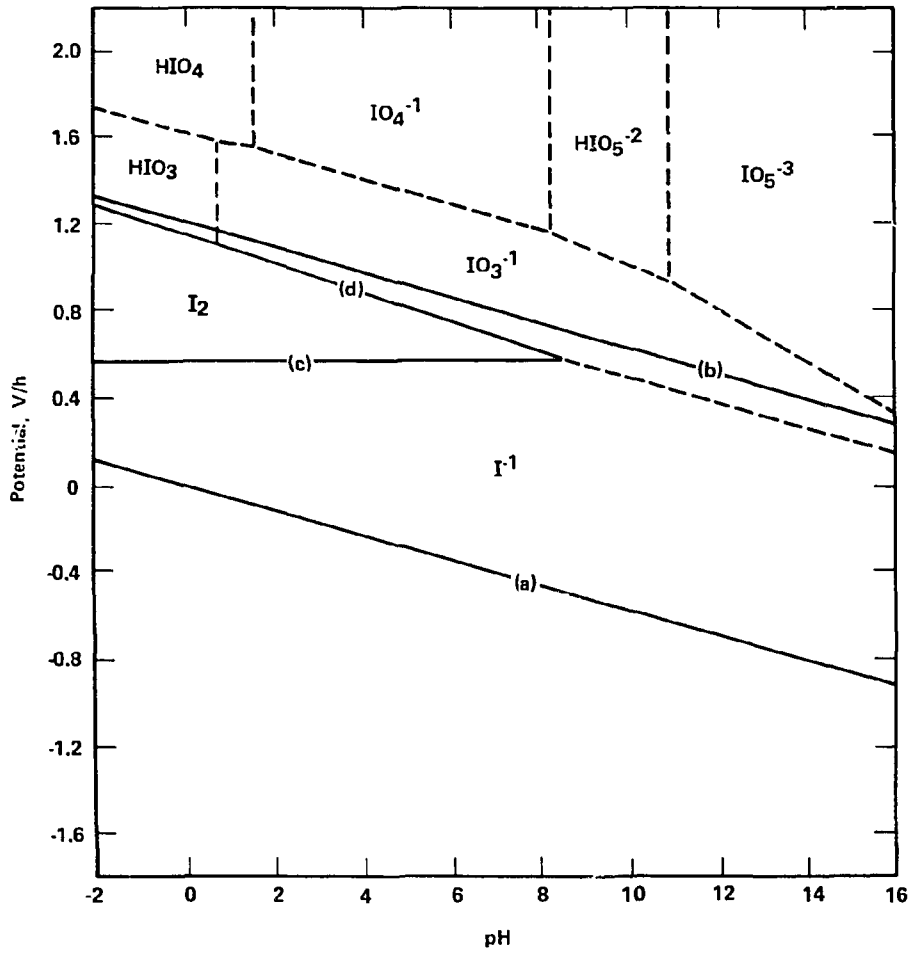

Fig. 3.15. Effect of aeration on the pH as a function of exposure time for a drop of distilled water containing 0.1 g of I_2 on Armco Iron and Nickel 201 surfaces.

that became liquid when exposed to air of normal humidity. Only uniform attack occurred during solid formation; however, once the liquid formed, severe localized attack was noted. Such conditions might occur in the voloxidizer off-gas system during an equipment outage.

The rate of attack also increased with increasing iodine concentrations at 25 and 40°C. However, severe attack occurred on the susceptible materials, even at the lowest iodine concentration evaluated (~2% of saturation).

The results of the studies indicate that the presence of HNO_3 and NO_2 can inhibit attack. For example, approximately 10^{-5} g/mL of NO_2 completely inhibited the pitting and weight loss of type 304L SS in air containing 1×10^{-5} g/mL of H_2O and 5.9×10^{-7} g/mL of I_2 at 25°C. Similarly, in tests with type 304L SS specimens located above boiling HNO_3, attack was inhibited when the HNO_3 concentration of the solution was 12 *M* or greater and the gas phase contained 7.4×10^{-7} g/mL of iodine. High water contents also inhibited attack, as demonstrated by tests performed on cooled type 304L SS specimens located above boiling 4 *M* HNO_3. Although quite effective on boldly exposed surfaces, none of the three methods effectively prevented attack in crevices.

Although the overall mechanism by which iodine attacks the susceptible stainless steels is not fully understood, a few conclusions can be made on the basis of the data generated. For example, the dominant reduction reaction probably is $I_2 \rightarrow 2I^- + 2e$ because the corrosion potentials for the unreactive titanium and Hastelloy C-276 were very close to the equilibrium potential for the iodine reduction reaction, as shown in Fig. 3.16. The corrosion process appears to be autocatalytic. Once the iodine forms, it probably promotes further attack of susceptible materials by disrupting the passive films. The metal iodides formed by the reaction are deliquescent, and, if sufficient moisture is present, a liquid phase forms that continues the attack. The iron and nickel ions generated by the corrosion reaction also appear to hydrolyze to produce very low pH values, further increasing the aggressiveness of the solution. Indeed, the very low pH values of the solutions on the surfaces of metals during rapid corrosion are probably the most puzzling aspect of the phenomenon because hydrolysis reactions for iron and nickel should not produce such low pH values. At present we are unable to explain the very low pH values that develop during the corrosion process.

One possible function of NO_2 and HNO_3 in inhibiting attack of the metals is readily apparent from the Pourbaix diagram.[6] These species tend to move the potential and pH into the region of stability for elemental iodine or IO_3^- and prevent the formation of iodides. In less humid environments, HNO_3 and NO_2 may also tie up water, thereby minimizing attack. Bloch et al.[7] speculate that such a mechanism is operative in the corrosion of austenitic stainless steel in liquid bromine. They postulate that NO_2 reacts with the water present to produce HNO_3 and HNO_2 according to the equation

$$2\,NO_2 + H_2O \rightarrow HNO_3 + HNO_2 \quad .$$

The HNO_3 then combines with any remaining water to form a trihydrate, thereby preventing the formation of HBr. A similar mechanism may be operable in the I_2-H_2O system.

The function of high water contents, such as occur under reflux conditions, in inhibiting attack is probably to dilute the aggressive iodide-containing solution on the metal surfaces

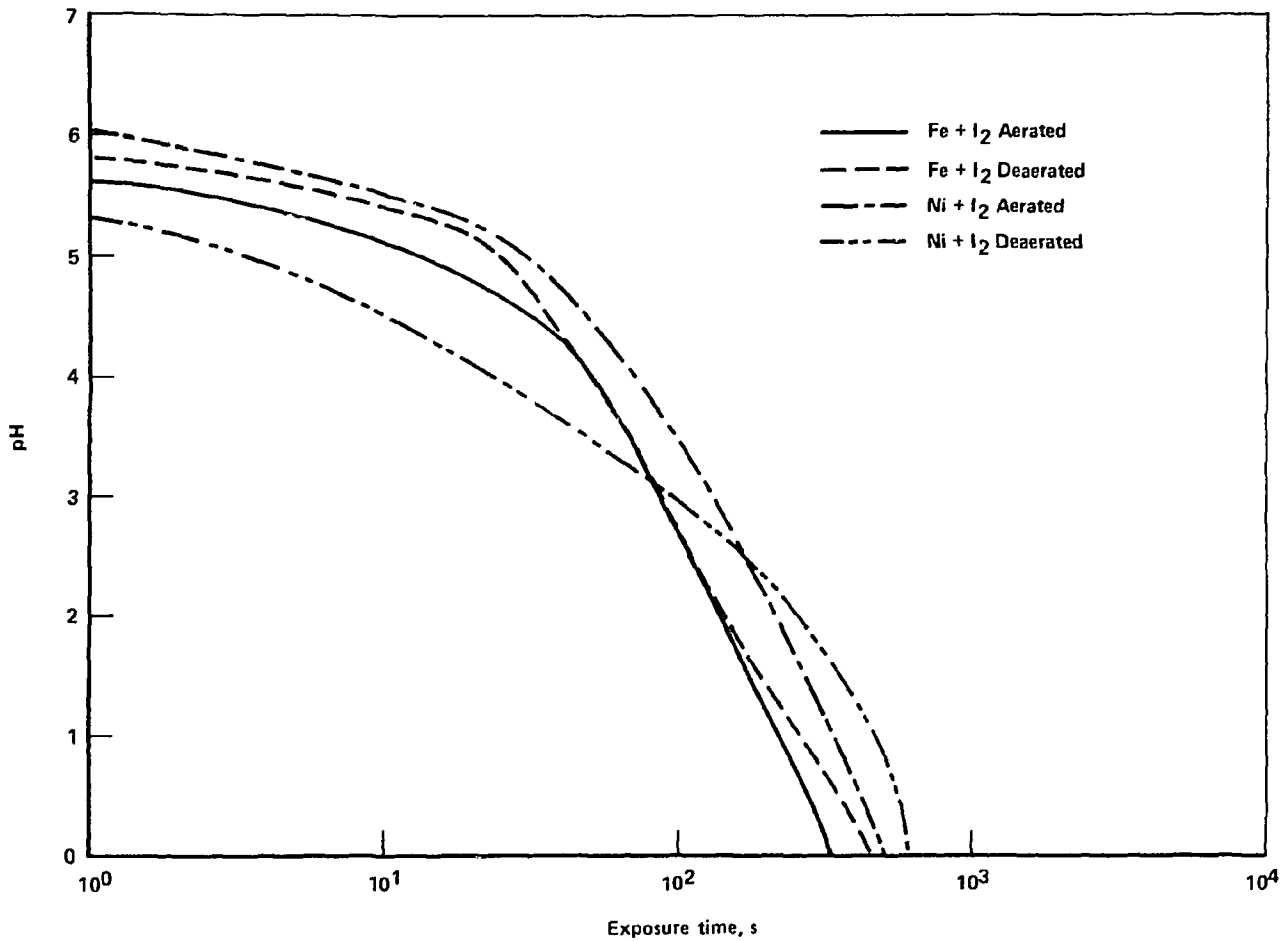

Fig. 3.16. Potential – pH diagram for the iodine-water system at 25°C for solutions containing 1 *M* iodine. (a) $2H^+ + 2e^- \rightarrow H_2$; (b) $O_2 + 4H^+ + 4e^- \rightarrow 2H_2O$; (c) $I_2 + 2e^- \rightarrow 2I^-$; (d) $2IO_3^- + 12H^+ + 10e^- \rightarrow I_2 + 6H_2O$.

before sufficient acidity forms to cause heavy attack. This explanation is supported by the tests performed in HI, where rates of attack of type 304L SS significantly decreased with decreasing HI concentration.

5. CONCLUSIONS

The following are our conclusions, based on the results of the experimental program.

1. The austenitic stainless steels and other iron- and nickel-based alloys that contain <6% molybdenum are rapidly pitted by elemental iodine in the presence of water vapor at room temperature and above.
2. Titanium, zirconium, and Hastelloy C-276 are resistant to attack by elemental iodine in the presence of water vapor.
3. The severity of attack increases with increasing iodine content of the vapors, but significant attack occurs even at very low iodine concentrations (≥2% of saturation).
4. Attack occurs at relative humidities well below saturation.
5. Rates of attack increase with increasing temperature at constant relative humidity but decrease with increasing temperature at constant water content in the vapor.
6. The severity of attack increases with increasing water content of the vapor except under conditions, such as reflux, where large amounts of water are present.
7. Concentrated HNO_3 and NO_2 are effective in inhibiting attack.
8. The inhibitors are relatively less effective in preventing corrosion in crevices than in preventing pitting on freely exposed surfaces.

REFERENCES

1. G. E. Creek and J. C. Griess, *Results of Corrosion Experiments Associated with Spent LMFBR Fuel Reprocessing*, ORNL/TM-3972 (October 1972).

2. L. Arbellot, "Behavior of Nickel and Its Alloys in the Presence of Halogens," *Corros. Anticorros.* 5, 112 (1957).

3. H. S. Mott, "Materials Selection Chart," *Chem. Eng.* 57(8), 197 (1956).

4. P. Weiland, private communication to J. C. Griess, Oak Ridge National Laboratory, August 1977.

5. *International Critical Tables* 3, 201, McGraw-Hill, New York, 1933.

6. M. Pourbaix, *Atlas of Electrochemical Equilibria*, National Association of Corrosion Engineers, Houston, 1974, p. 614.

7. M. R. Bloch et al., "Prevention of Corrosion of Stainless Steels by Br_2," *Corros. Sci.* 11, 453 (1971).